The Laplace-Beltrami operator: a ubiquitous tool for image and shape processing

Aaron Wetzler, Yonathan Aflalo, Anastasia Dubrovina, and Ron Kimmel

Technion - Israel Institute of Technology,
Haifa, Israel
{twerd,aflalo,nastyad,ron}@cs.technion.ac.il

Abstract. The ubiquity of the Laplace-Beltrami operator in shape analysis can be seen by observing the wide variety of applications where it has been found to be useful. Here we demonstrate a small subset of such uses with their latest developments including a scale invariant transform for general triangulated meshes, an effective and efficient method for denoising meshes using Beltrami flows via high dimensional embeddings of 2D manifolds and finally the possibility of viewing the framework of geodesic active contours as a surface minimization having the Laplace-Beltrami operator as its main ingredient.

Keywords: Laplace-Beltrami, denoising, scale invariant, active contours, segmentation

1 Introduction

The Laplace-Beltrami operator is a generalization of the Laplacian to non-flat Riemannian manifolds. The Laplacian operator appears in differential equations describing various physical phenomena, such as heat diffusion, wave propagation, etc. In computer vision it has been used extensively, for example for blob and edge detection, or image smoothing. When working with cruved manifolds, such as 3D shapes or even images represented as surfaces in 3D or 4D, like volume images, MRI or CT, we need a general representation of the Laplacian operator, such that it will take into account the non-trivial geometry of the manifold. There are many instances in the field of shape analysis where various types of metrics play an important role. The common approach presented in this article is to view the problem within a manifold processing framework, and use an appropriately defined metric in order to calculate the Laplace-Beltrami. Both heat diffusion over a surface as well as minimal surfaces are direct applications of the operator. More advanced methods involving this ubiquitous operator include the generation of various shape descriptors, diffusion distance definition, isometry invariant embedding, to name just a few. In this paper we analyze several such methods from the point of view of manifold processing and illustrate their inherent inter-connectivity.

2 Beltrami patch denoising

The Laplace-Beltrami is the generalization of the Laplacian on Riemanian manifolds. It has been shown [25] that image denoising can be effectively formulated by considering an image to be a 2D manifold embedded into a higher dimensional spatial-spectral space such as $\{x, y, R, G, B\}$. This embedding can then be traversed iteratively using the so called Beltrami flow which generates a scale space over the manifold and leads to noise reduction of the image while preserving relevant features such as edges.

More recent papers [23][28] have extended this approach by embedding the image manifold into a so called patch-space. The improved denoising capacity of these techniques, as well as their greater generality, suggests that the Beltrami flow is indeed well suited for dealing with the problem of depth map and image denoising. An example of the smoothing property of the Beltrami patch flow can be seen in Fig. 1.

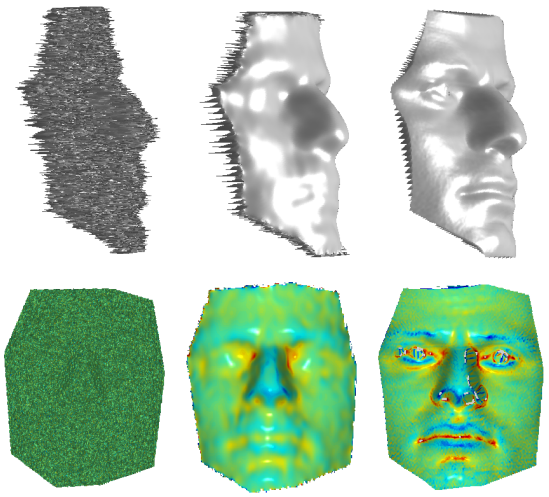

Fig. 1. Top row: Face with artificial Gaussian noise $\sigma = 10$, denoised using Beltrami patch denoising $PSNR = 42.45$, original face. Bottom row: Respective mean curvature of each face. It appears that despite the disruptive noise, the denoising process retains the main features present in the face.

2.1 Mathematical background

We consider a height field I to be a $2D$ Riemannian manifold embedded in a higher dimensional space. We thus define the patch-space mapping $P : \Sigma \rightarrow M \subseteq \mathbb{R}^{n(2w+1)^2+2}$ such that

$$P(x, y) = \left(x, y, \left\{I^k(x + i, y + j)\right\}\right) \quad , \tag{1}$$

for $i,j=-w,..,w, \quad k=1,..,n$ where $w\in\mathbb{N}$ is the window size and n is the number of channels we use. For the case of a single height field $n=1$, however if we were provided with a set of registered scans of a particular surface, n could represent the number of scans. The manifolds Σ and M are equipped with metrics G and H respectively. We require that lengths between corresponding points measured on each manifold are the same. For that end, we write that

$$ds^2=\left(dx\;dy\;dI^k_{i,j}\right)H\begin{pmatrix}dx\\dy\\dI^k_{i,j}\end{pmatrix}=(dx\;dy)\,G\begin{pmatrix}dx\\dy\end{pmatrix}. \tag{2}$$

where $I^k_{i,j}$ is the compact form for $\left\{I^k\left(x+iw,y+jw\right)\right\}$. In reality, the coordinates x and y do not possess the same physical measure as the intensity values of the height field so we need to introduce a scaling factor into the patch-space metric given by

$$h_{pq}=\begin{cases}\delta_{pq} & 1\leq p,q\leq 2\\ \beta^2\delta_{pq} & 2<p,q\leq n\left(2w+1\right)^2+2\end{cases}, \tag{3}$$

where δ_{pq} is the Kronecker delta. We can now use the chain rule $dI^k_{i,j}=\beta^2 I^k_{i,jx}dx+\beta^2 I^k_{i,jy}dy$ from which it follows that when we pullback the metric from the embedding the induced metric tensor is given by

$$G=\begin{pmatrix}1+\beta^2\sum_{i,j,k}{I^k_{i,jx}}^2 & \beta^2\sum_{i,j,k}I^k_{i,jx}I^k_{i,jy}\\ \beta^2\sum_{i,j,k}I^k_{i,jx}I^k_{i,jy} & 1+\beta^2\sum_{i,j,k}{I^k_{i,jy}}^2\end{pmatrix}. \tag{4}$$

Using this metric we define a measure S on the manifold. For a Euclidean embedding in M, S is none other than the area of the surface as measured in Σ

$$S\left[\Sigma,G\right]=Area\propto\iint\sqrt{\det(G)}dxdy, \tag{5}$$

where the proportion is up to a scale as a result of the non-unity coefficients of the diagonal entries of H. There is a more general version of the above measure called the Polyakov action which can be useful for non-Euclidean embeddings and details of its application to the Beltrami framework can be found in [25]. We minimize Eq. (5) using variational calculus and then multiply by $g^{-1/2}$ which is permitted through the freedom of paramaterization. We arrive at

$$\Delta_g I^k_{i,j}=\frac{1}{\sqrt{g}}\mathrm{div}\left(\sqrt{g}G^{-1}\nabla I^k_{i,j}\right)=0. \tag{6}$$

The left hand operator is recognized to be the Laplace-Beltrami operator and we can now compactly write the reformulation of the Beltrami flow in pach space as

$$I_t=\Delta_g I. \tag{7}$$

2.2 Method and results

The Beltrami flow in patch-space derived above can produce efficient and plausible denoising schemes in natural images. The flow is performed by a novel explicit update scheme. We fix the number of iterations and find the optimal β for a given σ in order to maximize the quantative efficacy of the process as measured by the Peak Signal to Noise Ratio $PSNR = 10\log_{10}\left(1/E\left[(I_{est} - I)^2\right]\right)$ across a wide range of different representative images. σ is the noise level assumed to be present in the image. It has been empirically observed that these two variables have a surprizingly simple relationship for natural images as seen in Fig. 2.

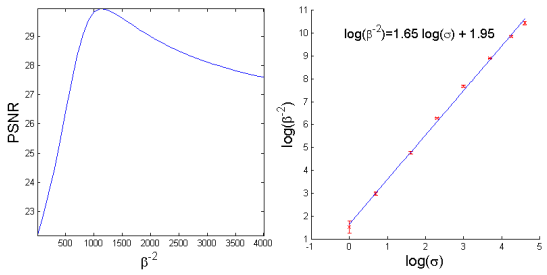

Fig. 2. Left: Example of $PSNR$ as a function of β^{-2} with a typical global maximum. Right: Linear relationship between the logarithms of σ and β^{-2}. Error bars indicate one standard deviation from the mean over a set of different images.

Accurate denoising of range images is often the first stage in 3D reconstruction pipelines that stitch depth images together to form a solid model and it is thus imperative that this process be fast and efficient. In our naive Matlab implementation we use an integral image and unit weighting of neighbouring height values to speed up the calculation of the flow update for each iteration. Furthermore, the diffusion update of every pixel in an image is independent of every other for a given iteration in our explicit scheme. This implies that an optimized implementation would need to take advantage of this inherrent parallelism and significant speed improvements could be expected. For implementation details of the method itself see [28].

Point clouds and meshes are often assumed to have noise which is Gaussian and that is offset along the normal direction to the true surface at every vertex location. In contrast, the noise model for range scanners is mainly observed to be offset in the direction of the capturing device's focal point. Furthermore the noise is not Gaussian in nature and also includes areas with missing data. This presents a significant hurdle for state of the art image denoising algorithms due to the fact that they are mostly tuned for optimal removal of additive white noise. A case in point is BM3D [13] to which we compare Beltrami patch denoising on a depth map obtained from a real scanner in Fig. 3.

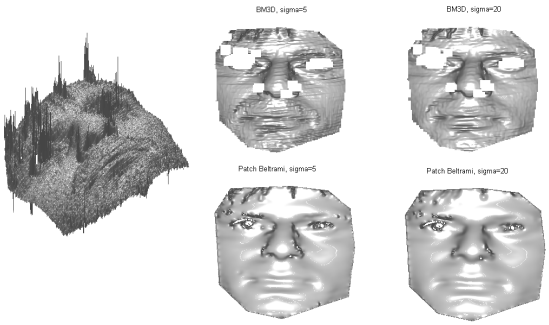

Fig. 3. Far left: Original noisy scan. Top row: BM3D for $\sigma = 5$ and $\sigma = 20$. Bottom row: Beltrami patch for $\sigma = 5$ and $\sigma = 20$.

Together with the efficiency of our method the Beltrami patch flow has an additional desirable property in that it can be tuned to eliminate weak high frequency structures. This is especially relevant for a variety of structured light scanners which tend to inject artifacts along the boundaries of the projected light patterns of the scanner. These artifacts can be observed as horizontal wrinkles in Fig. 3 and are faithfully preserved by BM3D whereas our method removes the artifacts while leaving the main components of the scan intact.

In this section we have illustrated the applicability of the Beltrami patch flow to height fields. One extension of this approach which is currently being investigated is how to apply the technique onto general meshes and point clouds. These data structures require a somewhat different treatment and a variety of new techniques are currently being developed by researchers to better understand and manipulate these discretized manifolds. With this in mind we now turn our attention to a new metric for use on triangulated meshes which is invariant to local changes in scale.

3 Invariant decomposition of the Laplace-Beltrami operator

In [26] it was argued that the Laplace-Beltrami operator and the corresponding heat operator acquire invariant properties when choosing an appropriately invariant metric. This observation was later exploited to construct an equi-affine invariant Laplace-Beltrami operator in [21] from which an invariant diffusion distance was extracted, and more recently in [1] where a scale invariant metric for surfaces was introduced.

At the other end, the standard Laplace-Beltrami operator's eigen-functions were used as a natural basis for shape representation, analogous to the Fourier basis in classical signal processing [16, 17]. We follow [21] and show how the re-

sults of [1] can be incorporated into the axiomatic world of shape processing.

One of the useful properties of the Laplace-Beltrami is that the operator admits a spectral decomposition. In this section we show how a new metric coupled with a discrete version of the Laplace-Beltrami and its eigenfunctions can be used to produce locally scale invariant signatures of shapes.

3.1 Introduction

Consider $S(u,v)$ a parametrized surface $S : \Omega \subset \mathbb{R}^2 \to \mathbb{R}^3$. The length of a parametrized curve C in S can be measured using a general parametrization p with

$$\begin{aligned} l(C) &= \int_{C\in S} ds = \int_C |C_p| dp = \int_C |S_u u_p + S_v v_p| dp \\ &= \int_C \sqrt{|S_u|^2 du^2 + 2\langle S_u, S_v\rangle du dv + |S_v|^2 dv^2}, \end{aligned} \tag{8}$$

from which we have the usual metric definition of infinitesimal distances on a surface

$$ds^2 = g_{ij} d\omega^i d\omega^j, \tag{9}$$

where we used Einstein summation convention, $\omega^1 = u, \omega^2 = v$ and $g_{ij} = \langle S_{\omega^i}, S_{\omega^j}\rangle$.

Using this convention and given a metric G on a manifold, we write the Laplace-Beltrami operator as

$$\Delta_G f = \frac{1}{\sqrt{g}} \partial_i \left(\sqrt{g} g^{ij} \partial_j f\right), \tag{10}$$

where g is the determinant of G, $g^{ij} = \left(G^{-1}\right)_{i,j}$, and ∂_i is the derivative with respect to the i^{th} coordinate.

The spectral theorem applied to the operator Δ_g states that it admits a spectral decomposition, i.e. an orthogonal eigenbasis $\{\phi_i, i \in \mathbb{Z}\}$ and a set of eigenvalues $\{\lambda_i, i \in \mathbb{Z}\}$ where

$$\Delta_g \phi_i = \lambda_i \phi_i, \quad \langle \phi_i, \phi_i \rangle = 1, \quad \forall i \in \mathbb{Z}. \tag{11}$$

This spectral decomposition has been extensively used for shape analysis. Diffusion geometry was introduced in [2] and refined in [12]. It uses the Laplace-Beltrami operator Δ_g of the surface as a diffusion or heat operator. The heat profile on the surface from a source located at s, after heat has dissipated for time t, is given by the heat kernel signature (HKS)[27, 6]

$$\text{HKS}(s,t) = \sum_i e^{-\lambda_i t} \phi_i^2(s) \tag{12}$$

where ϕ_i and λ_i are the corresponding eigenfunctions and eigenvalues of Δ_g, that satisfy $\Delta_g \phi_i = \lambda_i \phi_i$. The diffusion distance is then defined as

$$\begin{aligned} d^2_{g,t}(s,s') &= \|h_{s,t}(\hat{s}) - h_{s',t}(\hat{s})\|^2_g \\ &= \int_S (h_{s,t}(\hat{s}) - h_{s',t}(\hat{s}))^2 da(\hat{s}) \\ &= \sum_i e^{-2\lambda_i t}(\phi_i(s) - \phi_i(s'))^2. \end{aligned} \tag{13}$$

The choice of an appropriate metric that stays invariant to certain classes of deformations is important in the context of shape analysis. Several distances have been used, such as Euclidean [11, 3], geodesic [14, 19, 15, 18], diffusion [8], and affine invariant versions thereof [22] to compare and match between shapes. Yet another example is the scale invariant *HKS* [9] which is a non-linear function of the *HKS*. In order to be robust to local scale changes and isometries the following local scale-invariant isometric metric was proposed

$$\tilde{g}_{ij} = |K| \langle S_{\omega^i}, S_{\omega^j} \rangle, \tag{14}$$

so that

$$d\tau^2 = |K| \left(\langle S_u, S_u \rangle du^2 + 2\langle S_u, S_v \rangle du dv + \langle S_v, S_v \rangle dv^2 \right). \tag{15}$$

It is a similarity (local scale + isometry) invariant arc-length, where K is the gaussian curvature.

3.2 Experimental results

To demonstrate the robustness of the scale invariant metric with respect to local scale transformation, we first consider the shapes shown in Fig. 4. We then

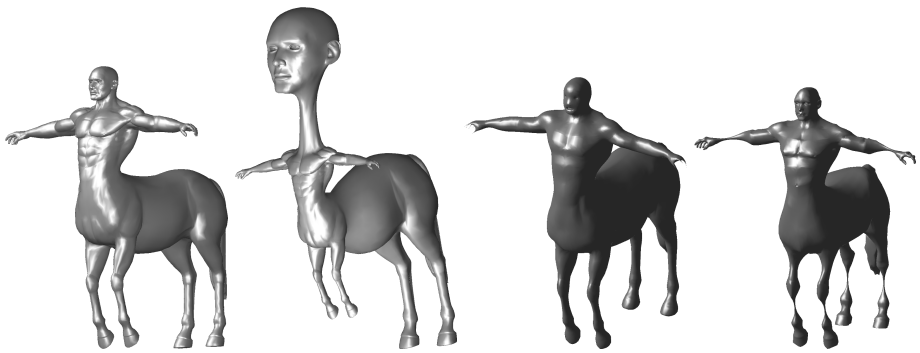

Fig. 4. Left to right: A centaur and its local scale transformed version. Details preservation for the coordinates reconstructed from the 1000 first eigenvectors of the Laplace Beltrami decomposition for the regular metric and the scale invariant metric.

present the profile of the heat kernel signature as a function of time (see Eq.

(12)) at three different points, the left hand finger tip, the right hand one, and the horseshoe of the front left leg as shown in Fig. 5. Another experiment that

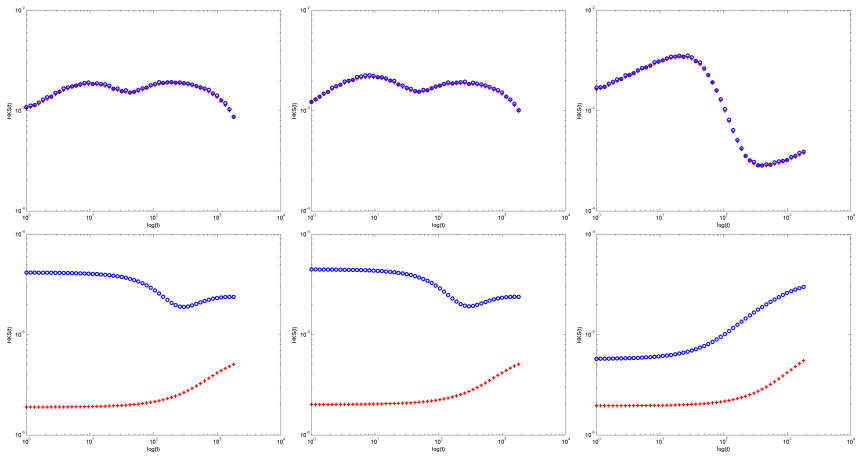

Fig. 5. Scaled heat kernel signatures for the regular metric (bottom), and the invariant version (top). The blue circles represent the signatures for three points on the original surface, while the red plus signs are computed from the deformed version. Using a log-log axes we plot the scaled-HKS as a function of t.

allows us to understand the importance of an invariant metric is done by the following eigen reconstruction of a shape. The eigenbasis of the shape has been studied in [17] and [16]. We compute the spectral decomposition of the Laplace-Beltrami with respect to both usual and scale invariant metric and compute an approximation of the original shape by projecting the coordinates of the shape on the first one thousand eigenvectors in that basis. We notice that the local scale invariant Laplace-Beltrami has a spectral decomposition that preserves details at all scales, and can be useful not only to analyze a group of shapes with local scale transfomations but also shapes whose small details are important as shown in Fig. 4. In the last experiment depicted in Fig. 6 we applied the GMDS algorithm [7] using local scale invariant diffusion distance to compute the correspondence between an armadillo and its scaled version

The Laplace-Beltrami's ubiquity can be seen not only in its application to shape understanding but also to the field of computer vision where its tendency towards minimal surfaces can be elegantly linked with the classic problem of segmentation through the geodesic active contours model.

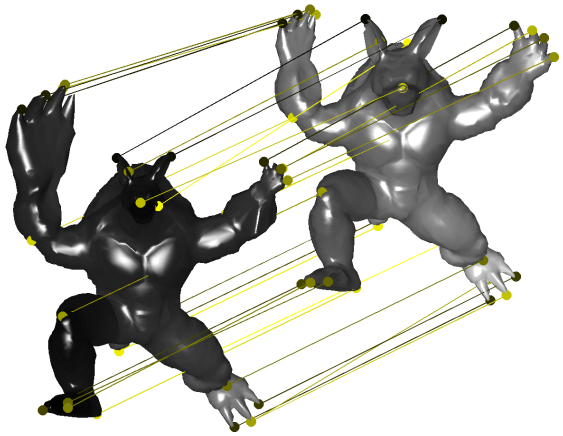

Fig. 6. Correspondences between the Armadillo and its local scale tranformed version using GMDS with the scale invariant metric.

4 Geodesic active contours and the Laplace-Beltrami framework

In this section the Laplace-Beltrami operator and the flow towards minimal surfaces that it generates is shown to be intimately related to the Geodesic Active Contours (GAC) model for image segmentation [10]. Related work include the papers by Bresson *et al.* [5], who showed how to obtain the GAC flow by minimizing a *weighted Polyakov action*, and Bogdanova *et al.* [4], who showed similar results for embedding spaces other than 3-D Euclidean space. Sochen *et al.* [24] examined the image filtering problem, and showed that there existed an intimate relationship between the PDE-based geometric approaches, derived from minimizing the Polyakov action with an appropriate metric, and non-linear filters of robust statistics.

We proceed by briefly describing the two frameworks - the geodesic active contours and the generalized minimal surface flow, and then provide a formulation in which their relationship becomes evident.

4.1 Geodesic active contours

Geodesic active contours were introduced for object boundary detection using active contours evolving in time according to the intrinsic measures of the image. In [10] it was shown that curve evolution using the geodesic active contours model is equivalent to finding minimal distance curves in a Riemannian space whose metric is defined by the intrinsic image measures mentioned above. Specifically, these are curves that minimize the following length measure

$$L_R := \int f\left(|\nabla I\left(C(q)\right)|\right)|C'(q)|\,dq = \int f\left(|\nabla I\left(C(s)\right)|\right)ds, \tag{16}$$

in a Riemannian space with the metric tensor $g_{ij} = f\left(|\nabla I\left(C\right)|\right)\delta_{ij}$. The function $f\left(|\nabla I\left(C\right)|\right)$ is an edge indicator function, designed to stop the active contour when it arrives to the object boundary.

Casseles *et al.* used steepest-descent method to minimize the length L_R (16), and obtained the following curve evolution flow

$$\frac{\partial C(t)}{\partial t} = \left(f(I)\kappa - \nabla f \cdot \boldsymbol{N}\right)\boldsymbol{N}, \tag{17}$$

where κ is the curvature of C, and $\boldsymbol{N}$ is its unit inward facing normal.

The level set formulation [20] of the geodesic problem (17) is given by

$$\begin{aligned}\frac{\partial u}{\partial t} &= |\nabla u|\,\mathrm{div}\left(f(I)\frac{\nabla u}{|\nabla u|}\right)\\ &= f(I)\,|\nabla u|\,\mathrm{div}\left(\frac{\nabla u}{|\nabla u|}\right) + \nabla f(I)\cdot\nabla u,\end{aligned} \tag{18}$$

where $u(x,y,t)$ is the level set function of the evolving curve - $C(x,y,t) = \{(x,y) : u(x,y,t) = 0\}$, and $\kappa = \mathrm{div}\left(\frac{\nabla u}{|\nabla u|}\right)$ gives the curvature of the level sets of the function u.

The level set function flow in Eq. (18) can be interpreted as a generalized minimal surface flow. In order to show this we will use the methodology described by Sochen *et al.* in [25], which we will review briefly in the following section.

4.2 Generalized minimal surface flow

Let us treat the level set function $u(x,y)$ as a two-dimensional surface embedded in a 3-dimensional space. As in Sec. 2 we define such an embedding by the map $\mathbf{X} : \Sigma \to M$, where Σ denotes a 2-D manifold Σ with local coordinates (σ_1, σ_2), and M denotes the 3-D embedding space M. Explicitly, $\mathbf{X}$ is written as $\mathbf{X} = \left(X^1(\sigma^1,\sigma^2), X^2(\sigma^1,\sigma^2), X^3(\sigma^1,\sigma^2)\right)$. Both manifolds Σ and M are equipped with metric tensors, $g_{\mu\nu}(\sigma^1,\sigma^2)$ and $h_{ij}(x^1,x^2,x^3)$, respectively. The map $\mathbf{X}$ and the metric h_{ij} can be used to construct the metric on Σ

$$g_{\mu\nu}(\sigma^1,\sigma^2) = h_{ij}(\mathbf{X})\partial_\mu X^i \partial_\nu X^j. \tag{19}$$

Here we keep the Einstein summation convention, following the original work of [25]. Next, the following weight functional can be associated with the map $\mathbf{X} : \Sigma \to M$

$$S\left[X^i, g_{\mu\nu}, h_{ij}\right] = \int d^m\sigma\sqrt{(g)}g^{\mu\nu}\partial_\mu X^i \partial_\nu X^j h_{ij}(\mathbf{X}), \tag{20}$$

where $g^{\mu\nu}$ is the inverse of the metric $g_{\mu\nu}$ (that is $g^{\mu\gamma}g_{\gamma\nu} = \delta_{\mu\nu}$), and g is the determinant of $\{g_{\mu\nu}\}$. This weight functional is called Polyakov action, and can also be viewed as a generalized area measure. A particular case of the Polyakov action has already been shown in Sec. 2, Eq. (5).

The minimal weight map (embedding) $\mathbf{X}$ can be obtained using steepest-descent. The gradient of the Polyakov action with respect to the embedding is

$$-\frac{1}{2\sqrt{g}}h^{il}\frac{\delta S}{\delta X^l} = \frac{1}{\sqrt{g}}\partial_\mu\left(\sqrt{g}g^{\mu\nu}\partial_\nu X^i\right) + \Gamma^i_{jk}\partial_\mu X^j\partial_\nu X^k g^{\mu\nu} \tag{21}$$

In order to find the minimal measure embedding, Sochen *et al.* [25] used the following gradient descent flow

$$X^i_t = -\frac{1}{2\sqrt{g}}h^{il}\frac{\delta S}{\delta X^l}. \tag{22}$$

We note that the gradient (21) was obtained by multiplying the Euler-Lagrange equations of (20) by a strictly positive function and a positive definite matrix, that together were called a $pre-factor$. It does not change the minimum, and produces a geometric parameterization-invariant flow. We will see that the pre-factor needed to produce the GAC flow will be somewhat different, stemming from the different geometry of the problem. We can also see that the first term in the right-hand side of the Eq. (21), $\frac{1}{\sqrt{g}}\partial_\mu\left(\sqrt{g}g^{\mu\nu}\partial_\nu X^i\right)$ is exactly the Laplace-Beltrami operator acting on the embedding X, denoted above by Δ_g. The second term includes the Levi-Civita connection coefficients Γ^i_{jk}, that describe the geometry of the embedding space. When $M = \mathbb{R}^3$ with Euclidean metric, $h_{ij} = \delta_{ij}$, the second term vanishes, and the flow becomes $X_t = \Delta_g X$, as seen in the previous sections.

4.3 Back to GAC: level set formulation as a flow toward minimal surface

Next, we show that the level set geodesic active contour flow in Eq. (18) can be obtained by minimizing a certain generalized area measure. First, let us choose X that maps a 2D Euclidean space ($\sigma^1 = x, \sigma^2 = y$) to a 3D Euclidean space, such that

$$\mathbf{X} = (x, y, u(x, y)). \tag{23}$$

The action functional we would like to study is

$$S = \iint dxdyf(|\nabla I(x, y)|)\sqrt{1 + |\nabla u|^2}, \tag{24}$$

This is Polyakov action obtained by choosing the following metric tensors for the parameter and the embedding spaces Σ and M, respectively

$$\begin{aligned} g_{\mu\nu} &= f(\sigma^2, \sigma^2)\left(\partial_\mu X \cdot \partial_\nu X\right), \\ h_{ij} &= f(x^1, x^2)\delta_{ij}. \end{aligned} \tag{25}$$

Both $g_{\mu\nu}$ and h_{ij} are legitimate metric tensors, and, since $(\sigma^2, \sigma^2) = (x, y)$ and $(x^1, x^2, x^3) = (x, y, z)$, Eq. (19) holds.

The metric tensor $g_{\mu\nu}$ written in a matrix form becomes

$$G = (g_{\mu\nu}) = f \begin{pmatrix} 1 + u_x^2 & u_x u_y \\ u_x u_y & 1 + u_y^2 \end{pmatrix} \tag{26}$$

The metric determinant is $g = \det(G) = f^2 \left(1 + \|\nabla u\|^2\right)$, and $\sqrt{g} = f\sqrt{1 + \|\nabla u\|^2}$. The inverse of the metric is

$$G^{-1} = (g^{\mu\nu}) = \frac{f}{g} \begin{pmatrix} 1 + u_y^2 & -u_x u_y \\ -u_x u_y & 1 + u_x^2 \end{pmatrix}. \tag{27}$$

Next, we use Eq. (21) in order to obtain the gradient-descent flow for the level set function component of $\mathbf{X}$, namely $X^3 = u(x, y)$,

$$u_t = X_t^3 = \frac{1}{\sqrt{g}} \partial_\mu \left(\sqrt{g} g^{\mu\nu} \partial_\nu u\right) + \Gamma_{jk}^3 \partial_\mu X^j \partial_\nu X^k g^{\mu\nu}. \tag{28}$$

Let us develop the two terms of the flow in Eq. (28) separately. Substituting the expressions for $\sqrt{g}$ and $g^{\mu\nu}$ into the first term of the right-hand side of the flow in Eq. (28) produces

$$\frac{1}{\sqrt{g}} \partial_\mu \left(\sqrt{g} g^{\mu\nu} \partial_\nu u\right) = \frac{1}{f\sqrt{1 + |\nabla u|^2}} \cdot \operatorname{div} \left(\frac{\nabla u}{\sqrt{1 + |\nabla u|^2}} \right) \tag{29}$$

In order to calculate the second term of the flow in Eq. (28) we must find the expression for the Levi-Civita connection coefficients Γ_{jk}^3. For the metric h_{ij} defined in Eq. (25)

$$\begin{aligned} \Gamma_{jk}^i &= \frac{1}{2} h^{il} \left(\partial_j h_{lk} + \partial_k h_{jl} - \partial_l h_{jk}\right) \\ &= \sum_l \frac{1}{2} \frac{1}{f} \delta_{il} \left(\partial_j \left(f \delta_{lk}\right) + \partial_k \left(f \delta_{jl}\right) - \partial_l \left(f \delta_{jk}\right)\right) \\ &= \frac{1}{2} \frac{1}{f} \left(\delta_{ik} \partial_j f + \delta_{ji} \partial_k f - \delta_{jk} \partial_i f\right) \end{aligned} \tag{30}$$

Therefore

$$\Gamma_{jk}^3 = \frac{1}{2f} \left(\delta_{3k} \partial_j f + \delta_{j3} \partial_k f\right), \tag{31}$$

or, in a matrix form,

$$\Gamma^3 = \frac{1}{2f} \begin{pmatrix} 0 & 0 & f_x \\ 0 & 0 & f_y \\ f_x & f_y & 0 \end{pmatrix}. \tag{32}$$

Finally, the second term of the flow from Eq. (28) becomes

$$\Gamma_{jk}^3 \partial_\mu X^j \partial_\nu X^k g^{\mu\nu} = \frac{\nabla f \cdot \nabla u}{f^2 \left(1 + |\nabla u|^2\right)}. \tag{33}$$

Using Eq. (29) and Eq. (33) we obtain the expression for the level set function flow

$$u_t = \frac{1}{f\sqrt{1+|\nabla u|^2}}\mathrm{div}\left(\frac{\nabla u}{\sqrt{1+|\nabla u|^2}}\right) + \frac{\nabla f \cdot \nabla u}{f^2\left(1+|\nabla u|^2\right)} \tag{34}$$

In order to obtain the GAC level set formulation we need to multiply the above flow by a pre-factor of $f^2\left(1+|\nabla u|^2\right)$. The flow obtained this way is

$$u_t = \mathrm{div}\left(f\frac{\nabla u}{\sqrt{1+|\nabla u|^2}}\right)\sqrt{1+|\nabla u|^2} \tag{35}$$

We see that, up to the additional constant 1, this is exactly the flow of the level set function of the geodesic active contours model from Eq. (18). Since the surface definition in Eq. (23) is arbitrary, we can choose the aspect ratio between du and dx, dy to be as large as we want. Thus 1 can be viewed as ε that vanishes upon the right selection of u.

Essentially what we have shown is that the geodesic active contours method in its level set formulation can be regarded as a minimal surface detection problem that minimizes the Polyakov action functional, and in doing so we have determined the related metric tensors for both parameter and embedding spaces.

5 Conclusions

We have shown the links between a patch based heat flow with the Beltrami operator as a diffusion filter, an invariant metric that was introduced into the operator yielding invariant geometries for shape matching and synthesis, and the geodesic active contour model expressed as a Beltrami diffusion equation. The Laplace-Beltrami operator acting on data in one form or another can be seen as one of the most fundamental operators in the analysis and processing of images and shapes. By manipulating the metric, the action and the filtering processes we have observed its applicability across a wide range of problems which further illustrates the inherent ubiquity of the operator. We believe that the Laplace-Beltrami viewpoint in this field has the potential to enable and enhance the understanding and exploration of images and shapes.

Acknowledgements

This research was supported by European Communitys FP7-ERC program, grant agreement no. 267414.

References

1. Y. Aflalo, D. Raviv, and R. Kimmel. Scale invariant geometry for non-rigid shapes. Technical report, Technion University, 2011.

2. M. Belkin and P. Niyogi. Laplacian eigenmaps for dimensionality reduction and data representation. *Neural Comput.*, 15(6):1373–1396, 2003.
3. P.J. Besl and N.D. McKay. A method for registration of 3-D shapes. *IEEE Transactions on Pattern Analysis and Machine Intelligence*, 14(2):239–256, 1992.
4. I. Bogdanova, X. Bresson, J. P. Thiran, and P. Vandergheynst. Scale space analysis and active contours for omnidirectional images. *Image Processing, IEEE Transactions on*, 16(7):1888–1901, 2007.
5. X. Bresson, P. Vandergheynst, and J. P. Thiran. Multiscale active contours. *Scale Space and PDE Methods in Computer Vision*, pages 167–178, 2005.
6. A. M. Bronstein, M. Bronstein, L. J. Guibas, and M. Ovsjanikov. Shape google: Geometric words and expressions for invariant shape retrieval. *ACM Transactions on Graphics*, 30(1), January 2011. Article 1.
7. A. M. Bronstein, M. M. Bronstein, and R. Kimmel. Generalized multidimensional scaling: A framework for isometry-invariant partial surface matching. *Proceedings of the National Academy of Science*, pages 1168–1172, 2006.
8. A. M. Bronstein, M. M. Bronstein, R. Kimmel, M. Mahmoudi, and G. Sapiro. A Gromov-Hausdorff framework with diffusion geometry for topologically-robust non-rigid shape matching. *International Journal of Computer Vision*, 89(2-3):266–286, 2010.
9. M. Bronstein and I. Kokkinos. Scale-invariant heat kernel signatures for non-rigid shape recognition. In *Proc. Computer Vision and Pattern Recognition (CVPR)*, pages 1704–1711, San Francisco, USA, 13-18 December 2010. IEEE Computer Society.
10. V. Caselles, R. Kimmel, and G. Sapiro. Geodesic active contours. *International journal of computer vision*, 22(1):61–79, February 1997.
11. Y. Chen and G. Medioni. Object modeling by registration of multiple range images. In *Proceedings of IEEE International Conference on Robotics and Automation*, volume 3, pages 2724 –2729, 1991.
12. R. R. Coifman and S. Lafon. Diffusion maps. *Applied and Computational Harmonic Analysis*, 21(1):5 – 30, 2006. Special Issue: Diffusion Maps and Wavelets.
13. K. Dabov, A. Foi, V. Katkovnik, and K. Egiazarian. Image denoising by sparse 3-d transform-domain collaborative filtering. *IEEE Transactions on Image Processing*, pages 2080–2095, 2007.
14. A. Elad (Elbaz) and R. Kimmel. On bending invariant signatures for surfaces. *IEEE Trans. on Pattern Analysis and Machine Intelligence (PAMI)*, 25(10):1285–1295, 2003.
15. M. Hilaga, Y. Shinagawa, T. Kohmura, and T.L. Kunii. Topology matching for fully automatic similarity estimation of 3D shapes. In *ACM SIGGRAPH 2001*, Los Angeles, CA, 12-17 August 2001.
16. Z. Karni and C. Gotsman. Spectral compression of mesh geometry. In *Proceedings of the 27th annual conference on Computer graphics and interactive techniques*, SIGGRAPH '00, pages 279–286, New York, NY, USA, 2000. ACM Press/Addison-Wesley Publishing Co.
17. B. Levy. Laplace-beltrami eigenfunctions towards an algorithm that "understands" geometry. *Conference on Shape Modeling and Applications, 2006. SMI 2006. IEEE International*, pages 13–13, 2006.
18. F. Mémoli and G. Sapiro. A theoretical and computational framework for isometry invariant recognition of point cloud data. *Foundations of Computational Mathematics*, 5(3):313–347, 2005.
19. R. Osada, T. Funkhouser, B. Chazelle, and D. Dobkin. Shape distributions. *ACM Transactions on Graphics*, 21(4):807–832, 2002.

20. S. Osher and J. A. Sethian. Fronts propagating with curvature-dependent speed: algorithms based on Hamilton-Jacobi formulations. *Journal of computational physics*, 79(1):12–49, 1988.
21. D. Raviv, A. M. Bronstein, M. M. Bronstein, R. Kimmel, and N. Sochen. Affine-invariant geodesic geometry of deformable 3D shapes. In *Computers and Graphics*, volume 35(3) of *Proceedings of Shape Modelling International (SMI'11)*, Herzliya, Israel, 22-24 June 2011. Elsevier.
22. D. Raviv, A. M. Bronstein, M. M. Bronstein, R. Kimmel, and N. Sochen. Affine-invariant geometry of deformable 3D shapes. In *Proc. of Computer vision and Pattern Recognition (CVPR)*. IEEE Computer Society, June 2011.
23. A. Roussos and P. Maragos. Tensor-based image diffusions derived from generalizations of the total variation and Beltrami functionals. In *ICIP*, September 2010.
24. N. Sochen, R. Kimmel, and A. M. Bruckstein. Diffusions and confusions in signal and image processing. *Journal of Mathematical Imaging and Vision*, 14(3):195–209, 2001.
25. N. Sochen, R. Kimmel, and R. Malladi. A general framework for low level vision. *IEEE Trans. on Image Processing*, pages 310–318, 1998.
26. Nir A. Sochen. Stochastic processes in vision: From langevin to beltrami. *Computer Vision, IEEE International Conference on*, 1:288, 2001.
27. J. Sun, M. Ovsjanikov, and L. J. Guibas. A concise and provably informative multi-scale signature based on heat diffusion. *Computer Graphics Forum*, 28(5):1383–1392, 2009.
28. A. Wetzler and R. Kimmel. Efficient beltrami flow in patch-space. In *Proceedings of the 3rd International Conference on Scale Space and Variational Methods in Computer Vision 2011*, volume 6667, pages 134–143. Springer, 2011.